12th Pacific Structural Steel Conference
Tokyo, Japan, November 9 -11, 2019

RESEARCH ON SEISMIC DESIGN OF DEEP WIDE-FLANGE STEEL COLUMNS IN THE U.S.

Chia-Ming Uang*, Gulen Ozkula and Piyachai Chansuk***

* University of California, San Diego
e-mails: cmu@ucsd.edu, pchansuk@eng.ucsd.edu

** Tekirdag Namik Kemal University
e-mail: gozkula@nku.edu.tr,

Keywords: moment resisting frames, seismic design, steel columns, local buckling, section compactness.

Abstract. *Designers in high seismic regions in the U.S. routinely use deep wide-flange columns for Steel Special Moment Frame design nowadays, a practice which deviates from that prior to the 1994 Northridge, California earthquake. This paper presents history of deep column issues that first surfaced in testing of moment connections, results from a numerical simulation that led to a comprehensive NIST-sponsored research program involving cyclic testing of more than 45 large-size columns. Findings from this program including implications to AISC Seismic Provisions will be presented.*

1 INTRODUCTION

Steel Special Moment Frame (SMF) composed of wide-flange beams and columns is a popular seismic force-resistance system in high seismic regions in the U.S. Prior to the Northridge, California earthquake in 1994, shallow columns with W12 or W14 columns [nominal depth = 12 in. (305 mm) or 14 in. (356 mm), respectively] are commonly used. For the past 15 years or so, however, designers have turned to deeper column sections (e.g., W24 and deeper sections) in order to meet the stringent story drift requirement specified in ASCE 7 [1] for economic considerations.

Story drift of an SMF is a function of the moment of inertia of the members. Refer to Figure 1 and Table 1 for an example of two column sections with a comparable moment of inertia; both sections meet the highly ductile requirement. The advantage of using the deeper W30×148 section is obvious because it is 65% lighter than that of the shallow W14×426 section. For SMF design with wide-flange members, the width-to-thickness ratios of the flanges ($\lambda_f = b_f/2t_f$) and web ($\lambda_w = h/t_w$) for a column cannot exceed the highly ductile limiting ratios, λ_{hd}, in accordance with the AISC Seismic Provisions, or AISC 341 [2]. For Intermediate Moment Frame (IMF) design, these limiting values can be relaxed to the moderately ductile limiting values, λ_{md}. See Table 2 for these limiting seismic compactness values.

Table 1 compares the width-thickness ratios of the sections and the member slenderness ratio, λ_L (= L/r_y) where L = column length and r_y = radius of gyration about the weak axis. Although both sections meet the highly ductile section requirement specified in the AISC Seismic provisions, or AISC 341 (AISC 2016), the slenderness ratios for both local and global buckling of the column are significantly higher. It is not clear if deep columns can develop comparable plastic deformations as those of shallow columns.

2 PAST RESEARCH ON CYCLIC BEHAVIOR OF STEEL COLUMNS

Prior to the Northridge earthquake, research on steel SMF was mainly focused on the wide-flange beam-to-column moment connections, especially the welded flange-bolted web connections, in the U.S. Following the strong column-weak beam design philosophy, SMF columns except for the panel zone regions were expected to remain elastic. Member sizes used for cyclic testing were "moderate" at most per the standard nowadays. Axial loads were not applied to the columns because it was difficult to do so, a challenging task which remains to be true even for modern structural testing laboratories. One notable study with applied column axial loads in beam-column subassemblage testing was conducted by Popov et al. [3]. Four specimens with columns oriented for strong-axis bending were tested. The column sizes were small (W8×28 and W8×48). The axial load remained constant, and the axial load ratio (P/P_y, where P_y = nominal yield strength of column) varied from 0.3 to 0.8. It was concluded from testing that the axial load ratio should be kept below 0.5 because a sharp drop in lateral strength, which was precipitated by flange local buckling and accompanied by a significant axial shortening, would occur at higher axial force levels.

Pseudo-dynamic testing of five first-story beam-column subassemblies was conducted by Schneider et al. [4]; the specimens were subjected to both axial compression and lateral drift. Two half-scale columns (W10×30 and W12×26) were investigated. For the W10×30 columns ($\lambda_f = 5.7$ and $\lambda_w = 29.5$), little local buckling was observed. For the slenderer W12×26 columns, both λ_w (= 47.2) and λ_f (= 8.5) were significantly larger than those of W10×30. All three specimens experienced significant local buckling at the column base.

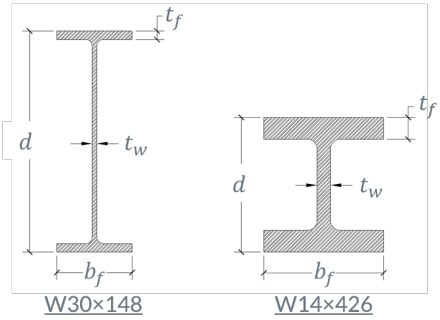

Figure 1. Comparison of Shallow and Deep Wide-flange Columns.

Table 1. Section Property Comparison of Shallow and Deep Wide-flange Columns

Section	I_x (×10³ mm⁴)	$b_f/2t_f$	h/t_w	L/r_y
W14×426	2,747	2.75	6.08	38.7
W30×148	2,780	4.44	41.6	73.7

L = 4,267 mm (14 ft) assumed.

Table 2. AISC Limiting Width-Thickness Ratios for SMF Columns

	Flange	Web
λ_{hd} for Highly Ductile Members	$0.32\sqrt{E/(R_yF_y)}$	when $C_a > 0.114$: $0.88\sqrt{E/(R_yF_y)}\,(2.68 - C_a) \geq 1.57\sqrt{E/(R_yF_y)}$ when $C_a \leq 0.114$: $2.57\sqrt{E/(R_yF_y)}\,(1 - 1.04C_a)$
λ_{md} for Moderately Ductile Members	$0.40\sqrt{E/(R_yF_y)}$	when $C_a > 0.114$: $1.29\sqrt{E/(R_yF_y)}\,(2.12 - C_a) \geq 1.57\sqrt{E/(R_yF_y)}$ when $C_a \leq 0.114$: $3.96\sqrt{E/(R_yF_y)}\,(1 - 3.04C_a)$

$C_a = P/(\phi P_y)$, where $\phi = 0.9$.

A significant number of full-scale moment connections were tested after brittle fracture of welded flange-bolted web moment connections was reported after the Northridge earthquake. The most notable study was that conducted by the SAC Joint Venture [5]. The focus of the study was on beam-to-column connections to ensure beam plastic hinging would occur while brittle fracture of welded joints was prevented. All except one conducted by Leon et al. [6] did not apply axial load to the columns. The testing conducted by the latter was to evaluate the effect of composite slab on brittle fracture of bottom flange weld, not the response of columns. The vast majority of the moment connection tests conducted in the SAC study also considered shallow (W12 or W14) columns to reflect a common practice prior to the Northridge earthquake. One exception was that conducted by Chi and Uang [7]. Three Reduced Beam Section (RBS) moment connections with W 27 columns were cyclically tested. Although no axial loads were applied to the columns, twisting of the column was observed, a phenomenon not previously reported when shallow columns were used. It was found that the twisting was caused by the eccentric beam flange force due to lateral-torsional buckling of the beam. It was also shown that the warping stress is highly dependent on the h/t_{cf}^3 ratio of the column section, where h = centerline distance between two flanges, and t_{cf} = flange thickness. For a given moment of inertia, it can be shown that a deep section (e.g., W27) has a h/t_{cf}^3 ratio significantly larger than that of a shallow section (e.g., W14). This is the first time that the concern of "deep column" surfaced. Since these specimens did not have a concrete slab, a follow-up study by Zhang and Ricles [8] demonstrated that the presence of a floor slab was effective in reducing twisting in the column. It was also reported through numerical simulation that axial load in the column has only a slight effect on connection performance.

The first comprehensive study on isolated wide-flange steel columns under cyclic axial load and lateral drift was conducted by Newell and Uang [9]. Shallow columns are widely used in braced frames because strength, not drift, usually dictates the member sizes. During an earthquake, steel braced frame columns can be subjected to cyclic high axial forces combined with inelastic rotation demand resulting from story drift. Cyclic testing of nine full-scale W14 column specimens (W14×132 to W14×370) representing a practical range of flange and web width-to-thickness ratios were subjected to different levels of axial force demand (35, 55, and 75% of P_y) combined with up to a story drift angle of 0.1 rad. No global buckling was observed in all test specimens. Flange local buckling was the dominant buckling mode. Specimens achieved story drift capacities of 0.07–0.09 rad. These large deformation capacities were, in part, achieved due to the delay in flange local buckling resulting from the stabilizing effect provided by the stocky column web (λ_w ranging from 6.9 to 17.7) of the W14 section specimens. Through finite element simulation, however, Newell and Uang [10] demonstrated that the cyclic behavior of deep columns (W27×146, W27×194, and W27×281) was characterized by a rapid strength degradation due to severe flange and web buckling interaction (see Figure 2). This study drew the attention of the engineering community on the cyclic response of deep columns in the U.S.

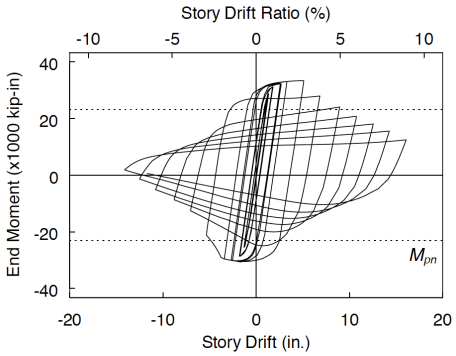

Figure 2. Predicted Response of a W27×146 Column [10].

In North America, Elkady and Lignos [11-12] investigated the cyclic behavior of deep columns (W16 to W36) through finite element simulation. The effect of axial load level, varying axial load, and loading sequence (symmetric loading and near-fault loading protocols) on flexural strength, plastic deformation capacity and axial shortening were reported. The first cyclic testing on deep columns was reported by Zargar et al. [13]; 1/8-scale models of a W36×652 column ($\lambda_w = 16.3$ and $\lambda_f = 2.5$) with a scaled length of 493 mm ($\lambda_L = L/r_y = 38$) were used for both monotonic and cyclic testing. Cyclic axial load was applied for all 4 cyclically tested specimens. Both lateral drift and end rotation were applied at the top end of the first-story column specimens. It was observed that lateral-torsional buckling was the dominant failure mode for all specimens. Although "deep" columns (in the sense it is a W36 section in prototype) were tested, it will be shown later that this section did not have the characteristics of deep columns because the width-thickness ratios were very small.

To address the deep column issue, National Institute of Standards and Technology (NIST) developed a comprehensive research plan in 2011 to study this issue at the member, subassemblage, and system levels [14]. The first step in implementing this plan was to evaluate experimentally the cyclic behavior of isolated deep columns. Test results will then be used by NIST to validate computational models and to improve seismic design provisions. Research at the member level, which started in 2013, was conducted at the University of California, San Diego. Findings from this research program are the focus of this paper. Parallel to this effort, a significant amount of research on deep columns was also conducted in North America. For example, researchers at the University of Michigan have performed extensive study using finite element simulation to investigate deep columns (e.g., [15, 16, 17]). Lignos and his associates have also conducted both numerical simulation and experimental testing of large-size deep columns (e.g., [18, 19]).

3 NIST RESEARCH PROGRAM

Parameters Investigated

Columns tested in this research were intended to represent the first-story columns in a multi-story SMF. Table 3 shows the test matrix; the numbers preceding the specimen labels indicate specimen groups. In the first phase of this test program, Ozkula et al. [20, 21] tested five W24 shapes (Groups 1 to 5) of ASTM A992 steel to investigate the effects of section and member slenderness parameters on the strong-axis flexural responses and buckling behavior. The applied axial force was kept constant in each test to simulate the response of an interior column. To study the effects of axial load levels on the failure mode, column ductility capacity, and axial shortening, each specimen group, with a few exceptions, comprised three specimens of the same shape undergoing low ($0.18P_y$), medium ($0.36P_y$), and high ($0.54P_y$) levels of axial compression; "L", "M", and "H" in the specimen designation indicate these axial load levels, respectively, in the specimen labels. Fully-restrained moment connections were used at both ends of the specimens; the intent was to simulate fixed-fixed boundary conditions.

Chansuk et al. [22] tested eleven additional wide-flange shapes (Groups 11 to 27) ranging from W14 to W30 in the second phase of the test program. The objectives were to (1) further examine the parameters investigated in the first phase testing, (2) determine whether findings from testing of W24 specimens in the first phase could be extrapolated to deeper (e.g., W30) and shallower (e.g., W14 and W18) shapes with similar section slenderness parameters, and (3) expand the experimental database. In addition, the effects of boundary conditions were investigated; fixed-rotating loading protocol was imposed to some specimens. Other parameters such as lateral drift loading sequences, and varying axial loads were also studied in this test program. See Figure 3 for the distribution of the width-thickness ratios of the sections tested in both phases.

Test Setup

Testing was conducted at the University of California, San Diego with a shake table test facility as shown in Figure 4. Specimens were tested in a horizontal position; L indicates their clear lengths (5490 mm for all except 5330 mm for Groups 11–13, 5380 mm for Groups 11–13, and 4270 mm for Groups 23–26). The west end of the specimens was connected to a reaction fixture that was fixed to a strong wall. The east (i.e., moving) end was connected to a reaction fixture that was tied down to the moving platen, simulating a column top end that swayed (and rotated for the fixed-rotating loading case) during a seismic event. With this test setup, longitudinal movements of the platen, which were force-controlled, imposed a targeted axial force, P, to the specimen. Applied (i.e., measured) cyclic lateral displacement, Δ_m, of the platen in the horizontal plane

Table 3. Test Matrix (Strong-axis Bending Specimens)

Group No.	Shape	Specimen Designation	Slenderness Ratios			Axial Load		Buckling Mode
			λ_f	λ_w	λ_L	C_a	P/P_y	
1	W24×176	1L 1M 1H	4.1	28.7	71.1	0.2 0.4 0.6	0.18 0.36 0.54	Coupled Buckling
2	W24×131	2Z 2L 2L-P 2M 2M-NF 2H	6.7	35.6	72.7	0.0 0.2 0.2 0.4 0.4 0.6	0 0.18 0.18 0.36 0.36 0.54	In-plane Plastic Hinging
3	W24×104	3L 3M 3H	8.5	43.1	74.2	0.2 0.4 0.6	0.18 0.36 0.54	
4	W24×84	4L 4M	5.86	45.9	110.8	0.2 0.4	0.18 0.36	Coupled Buckling
5	W24×55	5L 5LM 5M	6.94	54.6	161.2	0.2 0.3 0.4	0.18 0.27 0.36	Elastic LTB
11	W24×176	11M 11H-VA 11H-BC	4.81	28.7	71.05	0.4 0.6	0.36 Varies 0.54	Coupled Buckling
12	W30×261	12LM 12LM-P	4.59	28.7	61.19	0.3	0.27	
13	W30×173	13M 13M-BC	7.04	40.8	63.16	0.4	0.36	In-plane Plastic Hinging
14	W30×90	14L	8.52	57.5	103.35	0.2	0.18	
15	W18×192	15L	3.27	16.7	77.42	0.2	0.18	Coupled Buckling
16	W18×130	16M 16M-BC	4.65	23.9	80.0	0.4	0.36	
17	W18×76	17L	8.11	37.8	82.76	0.4	0.36	In-plane Plastic Hinging
21	W18×130	21M-VAU 21M-VAU-BC 21M-NF 21M-VAM	4.65	23.9	80.0	0.4	0.36	Coupled Buckling
22	W30×148	22L	4.44	41.6	94.7	0.2	0.18	
23	W18×60	23L	5.44	38.7	100.0	0.2	0.18	
24	W14×82	24L	5.92	22.4	67.7	0.2	0.18	In-plane Plastic Hinging
25	W14×53	25L	6.11	30.9	87.5	0.2	0.18	Coupled Buckling
26	W14×132	26LM 26LM-VAM	7.15	17.7	44.7	0.3 0 to 0.6	0.27 0 to 0.54	SFB
27	W24×84	27L	5.86	45.9	110.8	0.2	0.18	Coupled Buckling

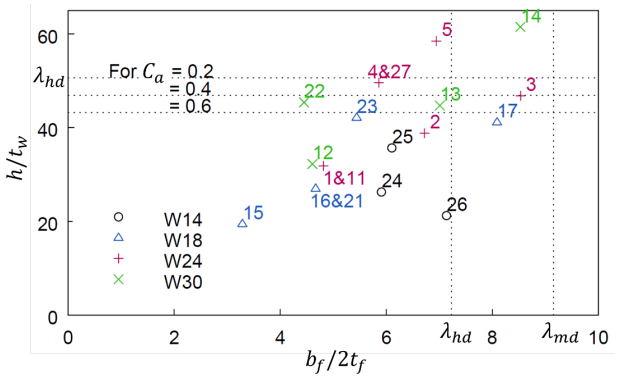

Figure 3. Distribution of Width-Thickness Ratios

imposed double-curvature, strong-axis bending to the specimens. Cyclic rotations, θ_m, of the platen about the member strong-axis simulated top end rotation of the first-story columns in an SMF. The platen was in a displacement-control mode for the lateral and strong-axis rotational movements.

Testing Procedure and Loading Protocols

Figure 5 shows the fixed-fixed and fixed-rotating boundary conditions used in this test program. An axial force was applied first in these tests and maintained at a targeted magnitude throughout the cyclic loading. For fixed-fixed tests, only cyclic lateral drifts were imposed at the moving end of the specimen, i.e., the top end of the first-story column in a moment frame in perspective. Typical in this test program, the symmetrical cyclic lateral-drift loading protocol for qualifying cyclic tests of beam-to-column moment connections in Special and Intermediate Moment Frames specified in Section K2.4b of AISC 341 [2] was used [Figure 6(a)]. Figure 6(b) shows the SAC near-fault loading sequence [23] that was used for a few specimens.

For specimens tested with the fixed-rotating boundary conditions, cyclic end rotations [Figure 5(b)] in-phase with and proportional to the AISC lateral drift sequence were also applied to the moving end of the column specimens. For this test program, the applied end rotations were expressed as follow: $\theta_m = \xi_m(\frac{\Delta_m}{L})$. Based on the results from nonlinear time-history analyses of an SMF, the value of ξ_m was set to 1 for all fixed-rotating specimens.

Data Correction Procedure for End Connection Flexibility

The objective of this test program was to evaluate the cyclic performance of isolated columns. Since it was very challenging to ensure full fixity at both ends for large-size column testing in laboratory setting, the effect of end connection flexibility [(Figure 4(b)] needs to be removed; this end flexibility has a significant effect on the initial stiffness of the response. Idealize the bolted-end connection as a rotational spring with a stiffness $K_\theta [= \beta(EI/L)]$. Treating the member as a Timoshenko beam-column that considers both the shear deformation and P-delta effects, the theoretical lateral stiffness is [24]:

$$K'_{11} = \frac{EIk^3\left[\sin kL - \frac{2P}{kLGA_s}(1-\cos kL)\right]}{2\left(1+\frac{P}{GA_s}\right)(1-\cos kL) - kL\sin kL} \qquad (1)$$

where $k = \sqrt{P/EI}$, G = shear modulus, and A_s = effective shear area. An example correction of the lateral force-story drift response of Specimen 13M with the fixed-fixed boundary condition is shown in Figure 7. The measured lateral stiffness, K_{me} (= 31.0 kN/mm), is 77% that of the theoretical value, K_e (= 40.5 kN/mm); the associated β value is 15.5. A procedure to correct the flexibility effect of fixed-rotating boundary condition is also reported in [24].

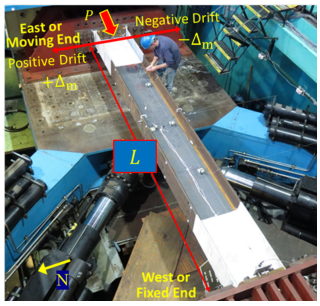

(a) Test Specimen Configuration

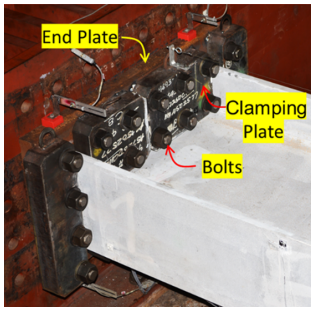

(b) Bolted Member Ends

Figure 4. Test Setup

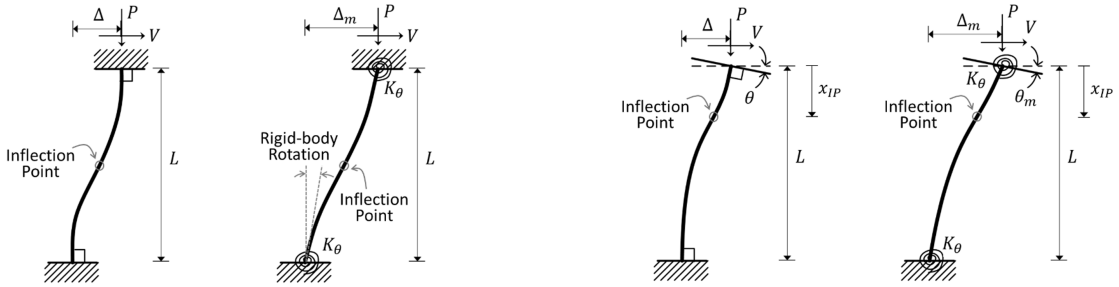

(a) Fixed-fixed Boundary Condition

(b) Fixed-rotating Boundary Condition

Figure 5. Boundary Conditions and End Connection Flexibility Effect.

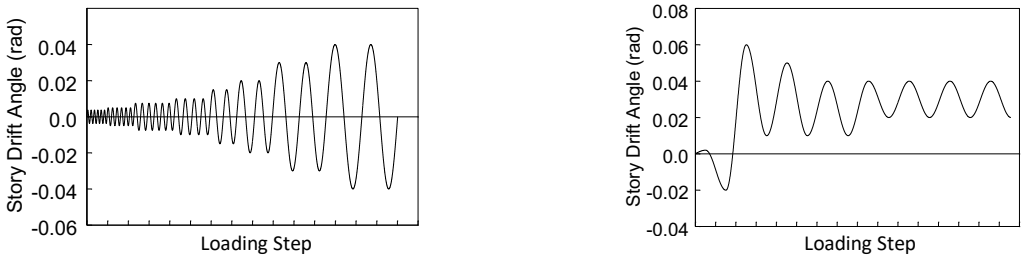

(a) AISC 341 Standard Loading Sequence (b) SAC Near-fault loading Sequence

Figure 6. Lateral Loading Sequences.

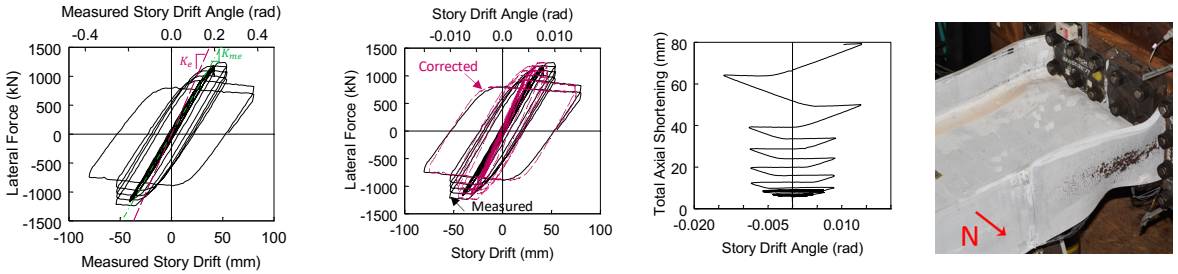

(a) Comparison of Initial Stiffnesses (b) Responses before and after Correction (c) Axial Shortening (d) Anti-symmetric Local Buckling

Figure 7. Response of Specimen 13M (Fixed-fixed Boundary Condition).

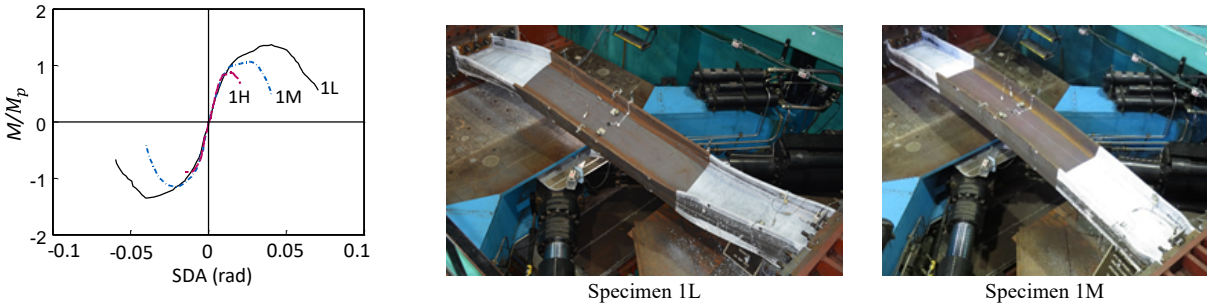

Specimen 1L Specimen 1M

(a) Comparison of Cyclic Backbone Curves (b) Coupled Buckling

Figure 8. Effect of Axial Force Level (Group 1 Specimens).

Typical Deep Column Responses

Hysteresis of the specimens is greatly influenced by beam-column yielding and buckling behavior, which are characterized into three main modes defined by Ozkula et al. [25]: (1) symmetric flange local buckling (SFB) mode, (2) anti-symmetric local buckling (ALB) mode, and (3) coupled buckling (CB) mode; see Figure 9(a) to (c). The first mode is usually observed in stocky shallow (e.g., W14 or shallower) columns with low h/t_w values; the web is effective to stabilize flanges such that flange local buckling with each flange buckles symmetrically with respect to the plane of the web is the dominant failure mode. Any occurs, web local buckling is very minor. When the value of h/t_w increases, as is the case of deep columns, latter two modes would dominate the response. Ozkula et al. also proposed a simple procedure to predict the governing buckling mode.

Figure 7(d) shows the anti-symmetric local buckling mode of Specimen 13M. FLB and WLB initiated simultaneously at 0.01 rad story drift angle, forming in-plane plastic hinges at both ends of the specimen. As a result, column axial shortening grew significantly [Figure 7(c)], and the member flexural strength degraded drastically. The cyclic backbone curves of Group 1 specimens (W24×176) are compared in Figure 8(a). Increasing the axial force level drastically reduced the inelastic deformation capacity of the column. All three specimens in this group failed in a coupled buckling mode involving significant lateral-torsional buckling in the out-of-plane direction [Figure 8(b)].

4 AXIAL SHORTENING

Of the three types of buckling mode mentioned above, both ALB and CB are accompanied by a significant axial shortening of the column (see Figure 9). Experimental results showed that axial shortening is affected by the magnitude and number of cycles, indicating that cumulative ductility needs to be considered. In this study, the cumulative ductility is measured by the normalized energy, η.

$$\eta = \frac{E_h}{M_p} \tag{2}$$

where M_p is the plastic moment capacity of the section, and E_h is the cumulative hysteretic energy computed as follows.

$$E_h = \int M_{end} d\theta \tag{3}$$

For the fixed-fixed case, M_{end} is the moment at the column end, and θ is the story drift tangle (*SDA*) in radians. The normalized axial shortening Δ_{axial} / L, of one plastic hinge is plotted against the normalized energy, η, for two sample fixed-fixed column specimens in Figure 10. The axial shortening at η = 0 corresponds to the elastic axial shortening due to the applied axial compression. The relationship between the normalized axial shortening and η can be expressed by the exponential form:

$$\frac{\Delta_{axial}}{L} = \alpha e^{\beta\eta} \tag{4}$$

where α is the elastic axial strain due to the constant axial compression given as

$$\alpha = \frac{P}{EA} \tag{5}$$

Parameter β for each specimen can be determined by curve fitting to measured data. A total of 19 data points from cyclic testing in this NIST project were evaluated. To enhance the database, an additional 96 numerically simulated cases were also considered [26]. Since the β value is a function of several parameters, including the magnitude of axial force as well as the section and member slenderness ratios, a stepwise multivariate regression analysis was performed to identify the most influential parameters. The regression analysis resulted in the expression for β given in Eq. (9).

$$\beta = C \left(\frac{h}{t_w}\right)^{1.56} \left(1 - \frac{P_u}{P_y}\right)^{-2.1} \tag{6}$$

where C is taken as 0.028 and 0.022 for ALB and CB, respectively. The coefficient of determination is R^2=93%.

Since typical software used by designers for performance-based seismic evaluation cannot simulate local buckling and axial shortening, it is postulated that, as an alternative to bypass this limitation, dissipated energy computed at the column ends by the software can be used with Eq. (4) to estimate buckling-induced axial shortening of deep columns.

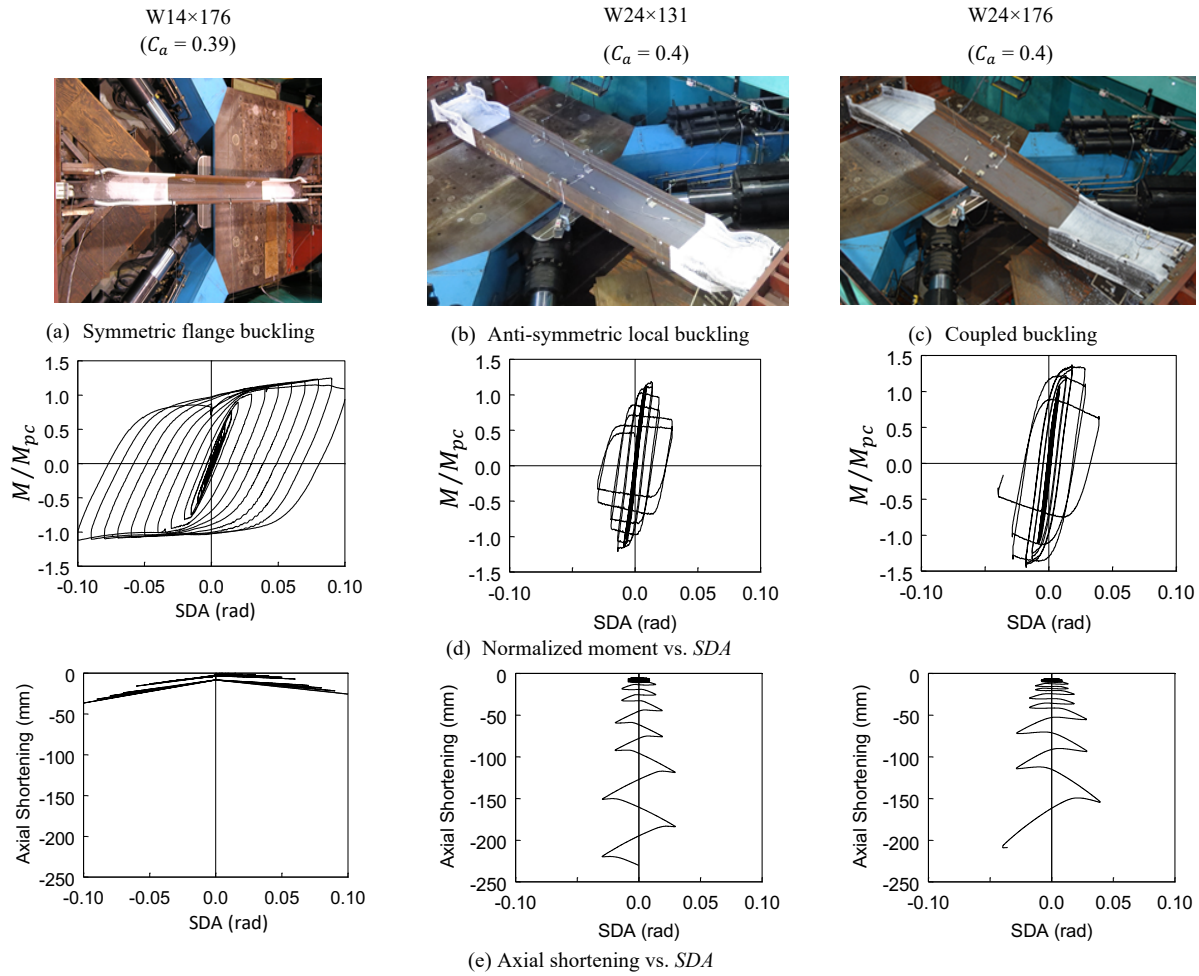

Figure 9. Column Cyclic Behavior and Axial Shortening of Different Failure Modes.

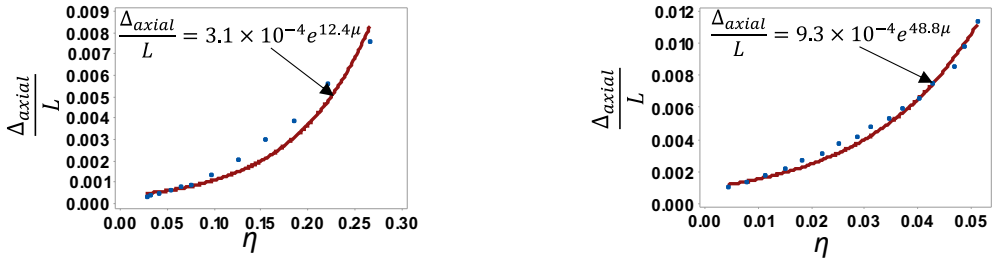

(a) Specimen 2L (b) Specimen 3H

Figure 10. Normalized Axial Shortening versus Normalized Cumulative Energy

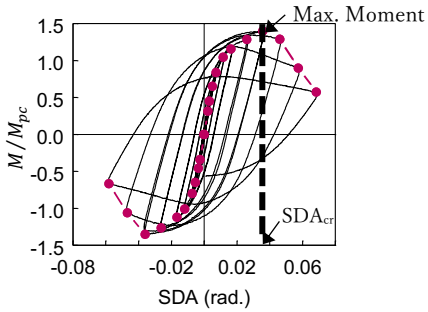

Figure 11. Definition of Critical Story Drift Angle (Specimen 1L)

5 SEISMIC COMACPTNESS REQUIREMENT

Both experimental testing and numerical simulation conducted in this research showed that wide-flange columns would experience significant buckling even though the cross section meets the AISC 341 highly ductile requirement for SMF design. Except for stocky, shallow sections, web and flange local buckling also interact each other. Such interactive local buckling triggers a significant degradation in flexural strength and large axial shortening. To avoid significant strength degradation, a procedure to establish the seismic compactness requirement is presented below.

Critical Story Drift Angle

Figure 11 shows the typical column response (a W24×176 column specimen with C_a = 0.2 and a fixed-fixed boundary condition that was subjected to the AISC loading sequence), where the end moment, normalized by the reduced plastic moment to account for the axial load effect, is plotted against the story drift angle, *SDA*. Since significant strength degradation and rapid growth of axial shortening would generally occur in deep columns after the maximum strength is reached, define the critical story drift angle, SDA_{cr}, as the lateral deformation capacity of the column at the peak strength (see Figure 11). Values of SDA_{cr} for 22 tested columns together with 550 numerically simulated columns were first determined. A multivariate regression analysis was then performed, resulting in the following expression with a coefficient of determination (R^2) of 0.82:

$$SDA_{cr} = 4.949 \times 10^{-2} \lambda_w^{-0.929} \left(1 - \frac{P_u}{P_{ya}}\right)^{2.126} \left(\frac{F_{ya}}{E}\right)^{-0.465} \tag{7}$$

Effective Critical Story Drift Angle

The critical story drift angle is affected by the boundary condition, cyclic loading sequence, and axial load type (constant or varying axial load). Therefore, Eq. (7) needs to be adjusted as follows:

$$SDA'_{cr} = \gamma \cdot SDA_{cr} \tag{8}$$

The adjustment factor γ is composed of three components:

$$\gamma = \gamma_b \gamma_l \gamma_a \tag{9}$$

where γ_b, γ_l, and γ_a are factors to account for the boundary condition, lateral loading sequence, and axial load type, respectively.

Table 4. Boundary Condition Effect

Specimen No.	SDA_{cr} (×0.01 rad)	$\frac{SDA_{cr}^{F\text{-}F}}{SDA_{cr}^{F\text{-}R}}$
1H	1.37	1.31
1H-BC	1.8	
13M	0.81	1.60
13M-BC	1.3	
16M	2.8	1.32
16M-BC	3.7	
	Average =	1.41

Table 5. Lateral Loading Protocol Effect

Specimen No.	SDA_{cr} (×0.01 rad)	$\frac{SDA_{cr}^{NF}}{SDA_{cr}^{AISC}}$
2M	1.35	1.20
2M-NF	1.89	
16M	2.88	1.52
21M-NF	5.9	
	Average =	1.36

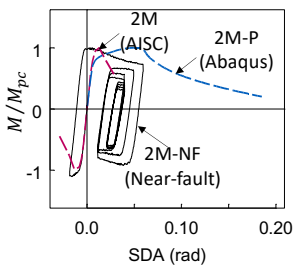

(a) W24×131 Specimens

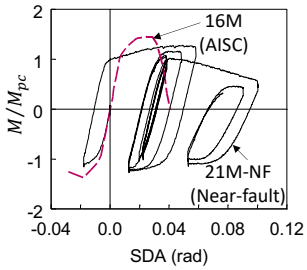

(b) W18×130 Specimens

Figure 12. Effect of Lateral Loading Sequence on Backbone Curves

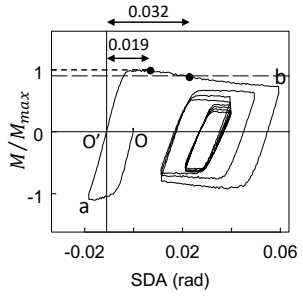

(c) Specimen 2M-NF

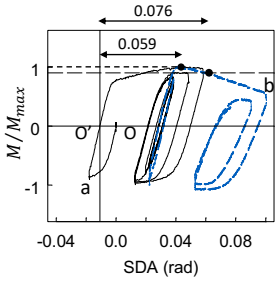

(d) Specimen 21M-NF

Figure 13. Determination of SDA_{cr} for Near-fault Loading Response

Boundary Condition Factor, γ_b

Eq. (7) was developed for the fixed-fixed boundary condition as shown in Figure 5(a). In reality, the top end of the first-story columns in an SMF would rotate with the story drift due to the flexibility of connected beams [Figure 5(b)]. Four pairs of specimens were tested with the fixed-fixed and fixed-flexible boundary conditions. It was assumed in testing that the rotating angle, θ, was equal to the imposed story drift angle. Table 4 summarizes the values of SDA_{cr} as defined previously. When the top end is allowed to rotate, the value of the fixed-rotating case ($SDA_{cr}^{F\text{-}R}$) is larger than that ($SDA_{cr}^{F\text{-}F}$) with the fixed-fixed boundary condition. With an average increase of 27% for four pairs of specimens, the value of γ_b is taken as 1.41.

Lateral Loading Sequence Factor, γ_l

Eq. (7) was developed with the AISC cyclic loading protocol [see Figure 6(a)]. Actual response of a frame column in a seismic event is not symmetric, and the response that leads to collapse tends to ratchet in one direction [27, 28]. In this test program, the near-fault loading sequence shown in Figure 6(b) was used to evaluate the ratcheting effect. Two pairs of nominally identical specimens (see Table 3) are used to evaluate the loading sequence effect. Figure 12 compares the cyclic backbone curve obtained from the AISC loading protocol with the near-fault loading response for each pair of specimens. [2M-P in Figure 12(a) is the computer simulated monotonic response.] In determining the SDA_{cr}^{NF} values (Table 5), the origin is shifted from O to O' as shown in Figure 13; the value of SDA_{cr}^{NF} reflects the effect of the initial excursion to -0.02 rad. Once the values for both AISC loading protocol (SDA_{cr}^{AISC}) and near-fault loading protocol (SDA_{cr}^{NF}) are determined, it is assumed that the ratcheting-type column response in an actual earthquake will be bounded by these two values, and the actual SDA_{cr} is taken as the average of the two. The ratio between this average value and SDA_{cr}^{AISC} is treated as γ_l:

$$\gamma_l = \frac{SDA_{cr}^{AISC} + SDA_{cr}^{NF}}{2(SDA_{cr}^{AISC})} \tag{10}$$

With the limited number of test data, the average value of γ_l is taken as 1.36.

Axial Loading Type Factor, γ_a

Most specimens in Table 3 were tested with the axial load maintained at a constant level; these specimens are representative of interior columns in a multi-story moment frame where the axial load remains relatively constant. But the axial load of exterior columns will fluctuate due to the overturning moment effect. Therefore, four specimens were tested with cyclic axial load to simulate the response of exterior columns. By applying the axial load cyclically, test results showed that the maximum lateral strength would increase relative to that loaded with a constant axial load. Local buckling was less severe, and the axial shortening was less. Therefore, the value of γ_a larger than 1.0 can be used to develop a limiting λ_w for highly ductile columns. For interior columns, which is the focus of this paper, the value of γ_a is taken as 1.0. The compactness requirement derived with γ_a = 1 will be conservative for the design of exterior columns.

Proposed Web Slenderness Ratios

Based on the information provided above, the value of γ equals

$$\gamma = \gamma_b \gamma_l \gamma_a = 1.41 \times 1.36 \times 1.0 = 1.92 \tag{11}$$

Eq. (11) together with Eq. (8) then becomes

$$SDA'_{cr} = 0.095\lambda_w^{-0.929}\left(1 - \frac{P_u}{P_{ya}}\right)^{2.126}\left(\frac{F_{ya}}{E}\right)^{-0.465} \tag{12}$$

where F_{ya} and P_{ya} are the actual yield stress and actual yield strength of the column. Solving λ_w from Eq. (12) gives the following:

$$\lambda_w = \frac{0.0794}{(SDA'_{cr})^{1.08}}\left(1 - \frac{P_u}{P_{ya}}\right)^{2.29}\sqrt{\frac{E}{F_{ya}}} \tag{13}$$

For code implementation in AISC 341, conservatively introduce a resistance factor ϕ_c (= 0.9) to the P_{ya} term. Furthermore, replace F_{ya} (actual yield stress) and P_{ya} (actual yield strength) by the following and re-define C_a for consistency with that defined in AISC 341-16:

$$F_{ya} = R_y F_y \tag{14a}$$

$$P_{ya} = R_y F_y A_g = R_y P_y \tag{14b}$$

$$C_a = \frac{P_u}{\phi_c R_y F_y A_g} \tag{14c}$$

where F_y = nominal yield stress, R_y = yield stress adjustment factor, and A_g = cross sectional area. Eq. (13) then becomes

$$\lambda_w = \frac{0.0794}{(SDA'_{cr})^{1.08}}(1 - C_a)^{2.29}\sqrt{\frac{E}{R_y F_y}} \tag{15}$$

For SMF design, AISC 341 Section E3.6b requires beam-to-column connections to accommodate a story drift angle of at least 0.04 rad. Setting SDA'_{cr} in Eq. (15) to 0.04 rad, the resulting λ_w, which is defined as λ_{hd} for highly ductile members in AISC 341, is

$$\lambda_{hd} = 2.54(1 - C_a)^{2.29}\sqrt{\frac{E}{R_y F_y}} \approx 2.5(1 - C_a)^{2.3}\sqrt{\frac{E}{R_y F_y}} \tag{16}$$

Similarly, equating SDA'_{cr} to 0.02 rad gives the limiting λ_{md} value for moderately ductile members in IMF design:

$$\lambda_{hd} = 5.35(1 - C_a)^{2.29}\sqrt{\frac{E}{R_y F_y}} \approx 5.4(1 - C_a)^{2.3}\sqrt{\frac{E}{R_y F_y}} \tag{17}$$

Figure 14 shows a comparison of the proposed web slenderness limits to those specified in AISC 341; the impact is more to SMF columns than to IMF columns. Also, the impact is much more significant at higher axial force levels for SMF columns.

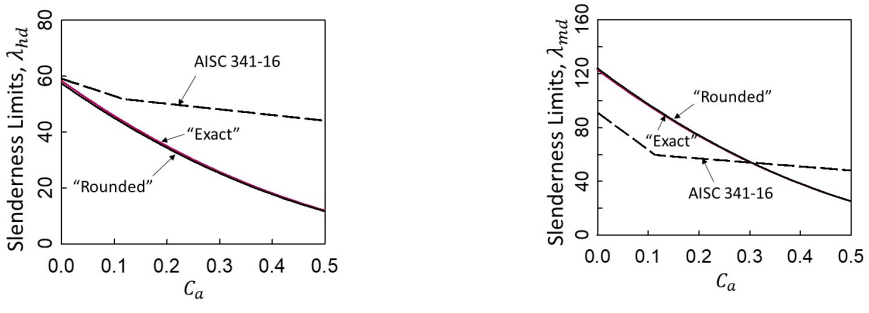

(a) SMF (b) IMF

Figure 14. Proposed and AISC 341 Web Slenderness Limits (A992 steel)

Limitations of Proposed Web Slenderness Limits

The above limiting web slenderness ratios should be applied with limitations. To assure adequate ductility in compression members with plastic hinges, for plastic design the design strength in compression should not exceed $0.75P_y$ per AISC 360 [29]. This plastic analysis requirement does not include the cyclic loading effect. For cyclically loaded columns, this limit is too relaxed. It is suggested that the C_a value be limited to 0.5, a value similar to that specified in ASCE 41 [30] to distinguish between columns with deformation-controlled and force-controlled actions.

Note that the fixed-fixed boundary condition provides a more critical, and hence conservative, condition for establishing the upper bound L/r_y value, beyond which global member buckling is more likely to occur. Both experimental and numerical simulation conducted in this research with this boundary condition showed that the L/r_y ratio did not significantly affect the column cyclic response as long as its ratio was not higher than 120. Since AISC 341 does not provides a limit on L/r_y, it is suggested that it be limited to 120.

6 CONCLUSIONS

Steel Special Moment Frame (SMF) built with wide-flange beams and columns is a popular seismic force-resistance system in the United States. To meet the stringent story drift requirement specified in the building code, design engineers turn to deep columns for economic considerations in the past two decades. Although AISC Seismic Provisions specify width-thickness limitations for both the flanges and web, deep column sections that meet these limitations usually have much higher width-thickness ratios, especially for the web, when compared to those if shallow columns (e.g., W14 and shallower sections) were used. Since higher slenderness ratios at the section and member levels would affect the stability characteristics of the columns, which are expected to form plastic hinges at the first-story column base, NIST initiated a comprehensive research program to address this issue. The first phase of this research program was to evaluate the cyclic performance of deep columns at the member level. More than forty large-size steel columns were tested under axial compression and cyclic lateral drifts at the University of California, San Diego. The following parameters were investigated: (1) width-thickness ratios of the section, (2) member slenderness, (3) axial force level, (3) constant axial load vs. cyclic axial load, (4) boundary condition (fixed-fixed vs. fixed-rotating), (5) lateral loading sequence (symmetric increasing-amplitude protocol, near-fault protocol, and monotonic loading), and (6) weak-axis bending and biaxial bending.

The much larger width-thickness ratio of the deep column web was not effective as in shallow (e.g., W14) and stocky columns to restrain and delay local buckling of the flanges; interactive flange and web local buckling was a typical buckling mode in deep column response. Such interactive buckling was accompanied by a significant axial shortening of the column. Local buckling together with out-of-plane lateral-torsional buckling was also observed in many tested deep columns that met the AISC compactness requirements for highly ductile members. Three types of buckling mode were identified: symmetric flange local buckling for shallow and stocky columns, anti-symmetric local buckling or coupled buckling involving out-of-plane buckling for deep columns.

A model that uses the dissipated energy to predict axial shortening of the column is presented. Based on the results from both cyclic testing and finite element simulation, a critical story drift angle beyond which significant strength degradation and axial shortening would occur was first established. This drift angle was then adjusted for the effects of boundary condition and lateral loading sequence to derive an effective critical story drift angle, which was used to derive web slenderness limits for both highly ductile members and moderately ductile members. It is shown that the AISC 341 limiting web compactness limits are not conservative and cannot avoid significant buckling and shortening at the first-story column base.

7 ACKNOWLEDGMENTS

Funding this research was provided by the Applied Technology Council under its Earthquake and Structural Engineering Research contract with the National Institute of Standards and Technology. Mr. J.O. Malley (Degenkolb Engineers) chaired the Project Advisory Committee. Mrs. A. Hortacsu (Applied Technology Council) served as the Project Manager. Dr. J. Harris (National Institute of Standards and Technology) provided technical guidance on this research. The authors would like to acknowledge the American Institute of Steel Construction for providing steel materials and The Herrick Corporation for providing fabrication of the test specimens.

REFERENCES

[1] ASCE, “Minimum design loads for buildings and other structures,” *ASCE/SEI 7*, Reston, VA, 2016.

[2] AISC, “Seismic provisions for structural steel buildings,” *ANSI/AISC 341-16*, American Institute of Steel Construction Chicago, IL, 2016.

[3] Popov, EP, Bertero, VV, and Chandramouli, S, “Hysteretic behavior of steel columns.” *Report No. EERC 75-11*, University of California, Berkeley, CA, 1975.

[4] Schneider, SP, Roeder, CW, and Carpenter, JE, “Seismic behavior of moment-resisting steel frames: experimental study,” *Journal of Structural Engineering*, ASCE, 119(6): 1885–1902, 1993.

[5] FEMA, “Recommended seismic design criteria for new steel moment-frame buildings,” *Report No. FEMA-355A*, Federal Emergency Management Agency, Washington, DC, 2000.

[6] Leon, RT, Hajjar, JF, and Gustafson, MA, “Seismic response of composite moment-resisting connections. I: performance,” *Journal of Structural Engineering*, ASCE, 124(8): 868-876, 1998.

[7] Chi, B and Uang, CM, “Experimental evaluation of reduced beam section connections to deep columns,” *Journal of Structural Engineering*, ASCE, 132(3): 346-357, 2006.

[8] Zhang, X and Ricles, JM, "Experimental evaluation of reduced beam section connections to deep columns," *Journal of Structural Engineering*, ASCE, 132(3): 346-357, 2006.

[9] Newell, JD and Uang, CM, "Cyclic behavior of steel wide-flange columns subjected to large drift," *Journal of Structural Engineering*, ASCE, 134(8): 1334-1342, 2008.

[10] Newell, JD and Uang, CM, "Cyclic behavior of steel columns with combined high axial load and drift demand," *Report No. SSRP-06/22*, Department of Structural Engineering, University of California, San Diego, 2006.

[11] Elkady, A and Lignos, DG, "Dynamic stability of deep slender steel columns as part of special MRSF designed in seismic regions: Finite element modelling," *Proc*., First International Conference on Performance-Based and Life-Cycle Structural Engineering, Hong Kong, China. 2012.

[12] Elkady, A and Lignos, DG, "Cyclic behavior of deep slender wide-flange steel beam-columns under combined lateral drift and axial load," *Proc*., 10th U.S. National Conference on Earthquake Engineering. EERI, Oakland, CA, 2014.

[13] Zargar, S, Medina, RA, and Miranda, E, "Cyclic behavior of deep steel columns subjected to large deformation demands and high axial loads," *Proc.*, 10th U.S. National Conference on Earthquake Engineering, EERI, Oakland, CA, 2014.

[14] NIST, "Research plan for the study of seismic behaviour and design of deep slender wide-flange structural steel beam-column members," *Report No. NIST GCR 11-917-13*, National Institute of Standards and Technology, Gaithersburg, MD, 2010.

[15] Fogarty, J and El-Tawil, S, "Collapse resistance of steel columns under combined axial and lateral loading," *Journal of Structural Engineering*, ASCE, 142(1), 2015.

[16] Fogarty, J, Wu, TY, and El-Tawil, S, "Collapse response and design of deep steel columns subjected to lateral displacement," *Journal of Structural Engineering*, ASCE, 143(9), 2017.

[17] Wu, TY, El-Tawil, S, and McCormick, J, "Highly ductile limits for deep steel columns," *Journal of Structural Engineering*, ASCE, 144(4), 2018.

[18] Elkady, A and Lignos, DG, "Analytical investigation of the cyclic behavior and plastic hinge formation in deep wide-flange steel beam-columns," *Bulletin of Earthquake Engineering*, 13(4): 1097–1118, 2015.

[19] Elkady, A and Lignos, DG (2018), "Full-scale testing of deep wide-flange steel columns under multiaxis cyclic loading: loading sequence, boundary effects, and lateral stability bracing force demands." *Journal of Structural Engineering*, ASCE, 144(2), 2018.

[20] Ozkula, G, Harris, J, and Uang, CM, "Observations from cyclic tests on deep, wide-flange beam-columns," *Engineering Journal*, AISC, 54(1):45–59, 2017.

[21] Ozkula, G and Uang, CM, "Seismic Behavior and Design of Deep, Slender Wide-flange Structural Steel Beam-Columns: Phase 1 Testing," *Report No. SSRP-15/06*, Department of Structural Engineering, University of California, San Diego, La Jolla, CA, 2015.

[22] Chansuk P, Ozkula, G, and Uang, CM, "Seismic Behavior and Design of Deep, Slender Wide-flange Structural Steel Beam-Columns: Phase 2 Testing," *Report No. SSRP-18/02*, Department of Structural Engineering, University of California, San Diego, La Jolla, CA, 2018.

[23] Clark, P, Frank, K, Krawinkler, H, and Shaw, R, "Protocol for fabrication, inspection, testing, and documentation of beam-column connection tests and other experimental specimens," *Report No. SAC/BD-97/02*, SAC Joint Venture, Sacramento, CA1997.

[24] Chansuk P, Ozkula G, and Uang CM, "Application of Timoshenko beam-column theory in data correction for steel beam-column," *Journal of Structural Engineering*, ASCE, 2019. (accepted)

[25] Ozkula G, Harris JL, and Uang CM, "Classifying cyclic buckling modes of steel wide-flange columns under cyclic loading." *Proc*., Structures Congress, ASCE, Denver, CO, 2017.

[26] Ozkula G, Harris JL, and Uang CM, "Buckling-induced shortening of deep W-shape columns in seismic steel frames," *Proc*., Eleventh U.S. National Conference on Earthquake Engineering, Los Angeles, CA, 2018.

[27] Suzuki, Y and Lignos, DG, "Development of loading protocols for experimental testing of steel columns subjected to combined high axial load and lateral drift demands near collapse." *Proc*., 10th National Conf. on Earthquake Eng., Anchorage, Alaska, 2014.

[28] Wu TY, El-Tawil S, and McCormick J, "Effect of drift loading history on the collapse capacity of deep steel columns," *Proc*., Structures Congress, ASCE, Denver, CO, 2017.

[29] AISC, "Specification for structural steel buildings*, ANSI/AISC 360-16*, American Institute of Steel Construction, Chicago, IL, 2016.

[30] ASCE, "Seismic evaluation and rehabilitation of existing buildings," *ASCE/SEI 41-17*, Reston, VA, 2017.